

The jets of AGN as giant coaxial cables.

Denise C. Gabuzda,¹ Matt Nagle¹ and Naomi Roche¹

Dept. of Physics, University College Cork, Cork, Ireland.
Email: d.gabuzda@ucc.ie

Received ; accepted

ABSTRACT

Context. The currents carried by the jets of active galactic nuclei (AGNs) can be probed using maps of the Faraday rotation measure (RM), since a jet current will be accompanied by a toroidal magnetic field, which will give rise to a systematic change in the RM across the jet.

Aims. The aim of this study is to identify new AGNs displaying statistically significant transverse RM gradients across their parsec-scale jets, in order to determine how often helical magnetic fields occur in AGN jets, and to look for overall patterns in the implied directions for the toroidal field components and jet currents.

Methods. We have carried out new analyses of Faraday RM maps derived from previously published 8.1, 8.4, 12.1 and 15.3 GHz data obtained in 2006 on the NRAO Very Long Baseline Array (VLBA). In a number of key ways, our procedures were identical to those of the original authors, but the new imaging and analysis differs from the original methods in several ways: the technique used to match the resolutions at the different frequencies, limits on the widths spanned by the RM gradients analyzed, treatment of core-region RM gradients, approach to estimation of the significances of the gradients analyzed, and inclusion of a supplementary analysis using circular beams with areas equal to those of the corresponding elliptical naturally weighted beams.

Results. This new analysis has substantially increased the number of AGNs known to display transverse RM gradients that may reflect the presence of a toroidal magnetic-field component. The collected data on parsec and kiloparsec scales indicate that the current typically flows inward along the jet axis and outward in a more extended region surrounding the jet, typical to the current structure of a co-axial cable, accompanied by a self-consistent system of nested helical magnetic fields, whose toroidal components give rise to the observed transverse Faraday rotation gradients.

Conclusions. The new results presented here make it possible for the first time to conclusively demonstrate the existence of a preferred direction for the toroidal magnetic-field components — and therefore of the currents — of AGN jets. Discerning the origin of this current-field system is of cardinal importance for understanding the physical mechanisms leading to the formation of the intrinsic jet magnetic field, which likely plays an important role in the propagation and collimation of the jets; one possibility is the action of a “cosmic battery”.

Key words. accretion, accretion disks—galaxies: active—galaxies: jets—galaxies: magnetic fields—magnetic fields

1. Introduction

Active galactic nuclei (AGNs) release vast amounts of energy, whose ultimate source is a supermassive black hole in the galactic nucleus. In so-called radio-loud AGNs, two relativistic jets of plasma emanate from the nucleus, presumably along the rotational axis of the black hole. The radio emission is synchrotron radiation, and can be linearly polarized up to about 75% in optically thin regions with uniform magnetic fields, with the polarization angle χ orthogonal to the projection of the magnetic field \mathbf{B} onto the plane of the sky (Pacholczyk 1970).

Very Long Baseline Interferometry (VLBI) yields radio images with very high resolution, corresponding to linear sizes of the order of a parsec at the typical distances of AGNs. A structure with a compact “core” at one end and a jet extending away from it predominates for radio-loud AGNs. The VLBI jets are virtually always one-sided, due to the relativistic aberration of the radiation in the forward direction of the jets’ motion: one jet approaches the Earth and is highly boosted, while the receding jet is highly de-boosted.

A theoretical picture of the basic nature of this core–jet structure was proposed by Blandford & Königl (1979), in which the “core” observed with VLBI corresponds to the “photosphere”

of the jet, where the optical depth is near unity, $\tau \approx 1$, and the jet material makes a transition from optically thick to optically thin. Although the orientation of the observed polarization angle rotates 90° to become parallel to the synchrotron \mathbf{B} field in sufficiently optically thick regions, this transition does not occur until an optical depth of $\tau \approx 6$, so that the polarized emission observed in all regions, including the VLBI core, is effectively expected to be optically thin (Cobb 1993, Wardle 2018).

Multi-frequency VLBI polarization observations provide information about the wavelength dependence of the parsec-scale polarization. One example is Faraday rotation occurring along the line of sight between the emitting region and the observer. Faraday rotation is a rotation of the observed linear polarization that arises when the associated electromagnetic wave passes through a region with free electrons and a non-zero \mathbf{B} field component along the line of sight. The simplest case corresponds to the situation when this mechanism operates in regions of “thermal” (non-relativistic or only mildly relativistic) plasma outside the emitting region, when the rotation is given by

$$\chi_{obs} - \chi_o = \frac{e^3 \lambda^2}{8\pi^2 \epsilon_0 m^2 c^3} \int n_e \mathbf{B} \cdot d\mathbf{l} \equiv RM \lambda^2, \quad (1)$$

where χ_{obs} and χ_o are the observed and intrinsic polarization angles, respectively, $-e$ and m are the charge and mass of the particles giving rise to the Faraday rotation, usually taken to be electrons, c is the speed of light, n_e is the density of the Faraday-rotating electrons, \mathbf{B} is the magnetic field, $d\mathbf{l}$ is an element along the line of sight, λ is the observing wavelength, ϵ_o is the permittivity of free space, and the coefficient of λ^2 is called the Rotation Measure, RM (e.g., Burn 1966). The action of such “external” Faraday rotation can be identified using simultaneous multifrequency observations, through its linear λ^2 dependence, allowing the determination of both the RM (which reflects the electron density and line-of-sight \mathbf{B} field in the region of Faraday rotation) and χ_o (the intrinsic direction of the source’s linear polarization, and hence the synchrotron \mathbf{B} field, projected onto the plane of the sky).

Many theoretical studies and simulations of the relativistic jets of AGNs have predicted the development of a helical jet \mathbf{B} field, which essentially comes about due to the combination of the rotation of the central black hole and its accretion disk and the jet outflow; Tchekovskoy and Bromberg (2016) provide a recent example. Researchers have long been aware that the presence of a helical jet \mathbf{B} field could give rise to a regular gradient in the observed RM across the jet, due to the systematic change in the line-of-sight component of the helical field (Perley et al. 1984, Blandford 1993). Statistically significant transverse RM gradients across the parsec-scale jets of an increasing number of AGNs have been reported in the literature over the past several years (Gabuzda et al. 2014, 2015b, 2017), and have been interpreted as reflecting the systematic change in the line-of-sight component of a toroidal or helical jet \mathbf{B} field across the jets (a helical \mathbf{B} field includes both toroidal and poloidal components; it is the toroidal component that gives rise to the transverse RM gradient). Basic physics leads to the conclusion that these jets carry currents, whose direction can be inferred from the direction of the toroidal \mathbf{B} field component giving rise to the transverse RM gradients.

Because the relativistic jets of AGNs are typically very narrow structures, it is important to verify that RM structures across jets that are not well resolved in the transverse direction are reliable. As has been discussed earlier by Gabuzda et al. (2015b), the Monte Carlo simulations of Hovatta et al. (2012), Mahmud et al. (2013) and Murphy and Gabuzda (2013) have demonstrated that, for RM maps made at wavelengths in the range 2–6 cm, the probability that an individual RM gradient with a significance of about 3σ or more is spurious is less than 1%, even when the observed width of the RM distribution across the jet is comparable to the resolution (beam size). These simulations also showed that RM gradients with significances of $2 - 3\sigma$ can also be considered trustworthy if they span at least two beam widths, or if they are observed at two or more epochs. In addition, simulated RM gradients remained visible even when the intrinsic jet width was much less than the beam width (Mahmud et al. 2013; Murphy and Gabuzda 2013).

These results led to a series of analyses (Mahmud et al. 2013; Gabuzda et al. 2014, 2015b, 2017) focusing on (i) monotonicity of the RM gradients, (ii) the range of values encompassed by the gradients relative to the uncertainties in the RM measurements and (iii) steadiness of the change in the RM values across the jet (ensuring an apparent “gradient” is not due only to values in a few edge pixels). These were taken to be the key factors in determining the trustworthiness of an RM gradient, that is, the probability that it is not spurious. These were all based on data obtained with the Very Long Baseline Array (VLBA) at various sets of frequencies between 4.6 GHz and 15.3 GHz, and include

both reanalyses of data for previously published RM maps and the publication of new RM maps. One key motivation for these studies was the need for a meaningful statistical analysis of the directions of the detected transverse RM gradients, that is, the directions of the toroidal \mathbf{B} -field components, and thus of the directions of the currents carried by AGN jets.

Table 1: Integrated RM values

Source	Taylor et al. (2009) Int. RM (rad/m ²)	Hovatta et al. (2012) Int. RM (rad/m ²)
0059+581	-175.4 ± 6.9	-64.7
0133+476	-101.2 ± 2.1	-75.3
0212+735	+21.8 ± 1.0	+9.7
0403-132	+7.1 ± 0.9	+7.8
0446+112	+19.4 ± 14.4	+21.9
0552+398	1.9 ± 5.5	-0.6
0834-201	-102.3 ± 8.7	+45
0859-140	17.0 ± 0.7	+1.3
0955+476	22.1 ± 4.0	+9.6
1124-186	-10.2 ± 7.7	-9.3
1150+812	80.6 ± 3.2	-19.4
1504-166	-26.4 ± 10.1	-11.2
1611+343	14.9 ± 0.7	+6.0
1641+399	18.0 ± 0.3	+19.4
1908-201	-73.3 ± 1.8	-20.4
2005+403	-171.4 ± 11.5	-40.0
2216-038	*	+0.6
2351+456	-31.3 ± 5.0	-33.5

* No entry is given for this RM by Taylor et al. (2009); the value given by Simard-Normandin et al. (1981) is -7 ± 9 rad/m², consistent with the value of Hovatta et al. (2012).

1.1. Outline of the paper

Section 2 describes the observations and data reduction procedures used, in particular how these are the same as and differ from those applied by Hovatta et al. (2012). The results are presented in Section 3, and discussed in Section 4. Our conclusions are summarized in Section 5.

2. Observations and data reduction

We carried out new analyses of the data used to produce the Faraday RM maps previously published by Hovatta et al. (2012). These observations were obtained at 8.1, 8.4, 12.1 and 15.3 GHz in 2006 on the NRAO Very Long Baseline Array (VLBA). The self-calibrated visibility data were downloaded from the MOJAVE project website¹; information about all steps of the calibration and initial imaging can be found in Hovatta et al. (2012).

We carried out the following aspects of our analysis in the same way as Hovatta et al. (2012):

Image alignment. We aligned the polarization-angle images at the different frequencies by determining the shifts between the corresponding intensity images required to align their optically

¹ <http://www.physics.purdue.edu/MOJAVE/>

Table 2: Map properties

Source	Peak (Jy/beam)	Lowest contour (%)	BMaj (mas)	BMin (mas)	BPA (deg)
0059+581	2.89	0.125	1.40	1.20	49.8
0059+581	2.88	0.125	1.30	1.30	0
0133+476	0.951	0.250	1.39	1.17	-4.7
0133+476	0.954	0.250	1.28	1.28	0
0212+735	3.01	0.250	1.28	1.22	43.8
0212+735	3.01	0.250	1.25	1.25	0
0403-132	1.38	0.250	2.49	1.03	0.5
0403-132	1.37	0.250	1.60	1.60	0
0446+112	1.61	0.250	2.15	1.03	-1.5
0446+112	1.66	0.250	1.49	1.49	0
0552+398	3.36	0.125	1.56	1.13	-3.0
0552+398	3.45	0.125	1.33	1.33	0
0834-201	2.78	0.250	2.79	0.87	-3.3
0834-201	2.98	0.250	1.56	1.56	0
0859-140	0.627	1.00	2.91	1.01	-5.7
0859-140	0.601	1.00	1.71	1.71	0
0955+476	1.43	0.250	1.48	1.21	1.7
0955+476	1.44	0.250	1.34	1.34	0
1124-186	1.26	0.250	2.90	0.94	-2.7
1124-186	1.26	0.250	1.65	1.65	0
1150+812	1.36	0.250	1.22	1.16	3.1
1150+812	1.36	0.250	1.19	1.19	0
1504-166	0.981	0.250	2.79	0.86	-4.3
1504-166	0.868	0.500	1.55	1.55	0
1611+343	3.58	0.500	1.64	1.14	1.5
1611+343	3.54	0.500	1.37	1.37	0
1641+399	1.99	0.500	1.59	1.15	4.7
1641+399	2.06	0.500	1.35	1.35	0
1908-201	2.80	0.250	2.68	0.93	1.4
1908-201	2.82	0.250	1.58	1.58	0
2005+403	0.843	0.500	1.78	1.26	21.4
2005+403	0.863	0.500	1.50	1.50	0
2216-038	1.852	0.250	2.42	0.98	-4.7
2216-038	1.854	0.250	1.54	1.54	0
2351+456	0.978	0.500	1.60	1.12	18.5
2351+456	1.005	0.500	1.34	1.34	0

thin regions, in our case using a cross-correlation method (Croke & Gabuzda 2010).

Treatment of polarization-angle calibration errors. We did not include the systematic errors due to the absolute polarization-angle calibration when searching for significant RM gradients, since these cannot give rise to spurious RM gradients (Mahmud et al. 2009, Hovatta et al. 2012).

Error estimation. We applied the improved error estimation formula of Hovatta et al. (2012) to determine the uncertainties in the polarization angles in individual pixels.

Treatment of Galactic Faraday Rotation. We took into account the estimated Faraday rotation occurring in our own Galaxy in the direction toward a source when significant, in order to better estimate the RM distribution in the immediate vicinity of the source.

Our imaging and RM analysis differs from that of Hovatta et al. (2012) in the following ways:

Technique used to match resolution. Hovatta et al. (2012) edited out the shortest baselines at the higher frequencies and the longest baselines at the two lower frequencies and used only the range of baselines common to all four datasets. In contrast, because the range of frequencies analyzed is not large, we used all available baselines, but ensured that the images at the different frequencies were compared using a common beam (corresponding to the lowest frequency).

Widths spanned by RM gradients. Hovatta et al. (2012) only searched for transverse RM gradients in RM distributions spanning more than about 1.5 beamwidths across the VLBI jet. Guided by the Monte Carlo simulation results described above (Hovatta et al. 2012, Mahmud et al. 2013, Murphy & Gabuzda 2013), we placed no formal limit on the width spanned by an RM gradient (although in practice only 4 of the 18 significant RM gradients we have detected are less than 1 beam width, and all are greater than 0.75 beam widths).

Treatment of core-region RM gradients. Hovatta et al. (2012) did not consider potential transverse RM gradients in the vicinity of the VLBI core, on the grounds that this region was at least partially optically thick, increasing the possibility of spurious gradients. This issue has been discussed in a number of recent studies (Motter & Gabuzda 2017, Gabuzda et al. 2017, Wardle 2018). Because the expected 90° “flip” in the polarization angle in the transition from the optically thin to the optically thick regime does not occur until an optical depth of $\tau \approx 6$, which is far upstream of the observed VLBI core region, there is no reason to expect severe departures from a linear λ^2 law for the Faraday rotation in the vast majority of cases, and we, like a number of earlier studies (Gabuzda et al. 2014, 2015b, 2017; Motter & Gabuzda 2017), therefore analyzed core-region RM gradients in the same way as those located in the jet, having verified an absence of appreciable deviations from a λ^2 law.

Estimation of significance. Hovatta et al. (2012) took the significance of an RM gradient to be the absolute value of the difference in RM values at the two ends of the gradient divided by the largest RM error at the edge of the jet (without including the systematic error due to the absolute polarization-angle calibration, which cannot give rise to spurious RM gradients, as was noted above (Mahmud et al. 2009, Hovatta et al. 2012)). We used a somewhat more conservative approach to calculating the significance of gradients, by comparing the absolute value of the RM difference across a gradient with the square root of the sum of the errors on the two RM values added in quadrature:

$$\sigma = \frac{|RM_1 - RM_2|}{\sqrt{\sigma_1^2 + \sigma_2^2}}. \quad (2)$$

Roughly speaking, our significances will usually be lower than those of Hovatta et al. (2012), by up to about a factor of $\sqrt{2}$. We note that in both of these approaches, the RM values considered will be near the edges of the RM maps, where the uncertainties are highest, so that both approaches are inherently conservative.

Supplementary analysis using circular beams. We considered versions of all the RM maps convolved using circular beams with areas equal to those of the natural-weighted elliptical beams (i.e., the radius of the circular beam was $R = \sqrt{(BMAJ)(BMIN)}$, where *BMAJ* and *BMIN* are the major and minor axes of the elliptical beam), as has been discussed in some earlier studies (Gabuzda et al. 2017, Motter & Gabuzda 2017). This helped test the robustness of gradients present in the RM maps made using the elliptical beams, and in some cases helped clarify the direction of a gradient relative to the local jet direction.

The observed Faraday rotation occurs predominantly in two locations: in the immediate vicinity of the AGN and in our own Galaxy. The latter “Galactic” RM must be estimated and removed if we wish to identify Faraday rotation occurring in the vicinity of the AGN itself. Low-resolution, low-frequency integrated RM measurements will generally be dominated by this

Galactic RM component, which is uniform across the source on milliarcsecond scales, and it is usually supposed that such low-frequency, low-resolution (compared to the VLBI images) integrated RM measurements provide a good estimate of the Galactic RM, although they will formally include some contribution from plasma in the vicinity of the source as well. Consistent with the approach adopted in the previous studies considered here (Gabuzda et al. 2014, 2015b, 2017), we used the integrated RM measurements of Taylor et al. (2009) at the positions of the sources considered directly; these values, given in Table 1, are based on the VLA Sky Survey (NVSS) observations at two bands near 1.4 GHz. The integrated RMs for most of these AGNs are low, less than about 30 rad/m^2 in absolute value; this is smaller than the typical uncertainties in the RM values measured in our maps, and we did not remove the effect of these small integrated RM values. Six of the objects have higher integrated RMs, ranging in absolute value from 80 rad/m^2 to 175 rad/m^2 , and we removed these integrated RMs from all values in the RM maps for these two sources. We note that this procedure is slightly different to the approach of Hovatta et al. (2012), who removed the average RM from the vicinity of the source on the sky based on the overall RM image of Taylor et al. (2009), rather than the value at the position of the source itself. This leads to small differences in the ranges of our RM maps for these six sources compared to the previously published RM maps (Hovatta et al. 2012), although the maps are very similar overall. The Galactic RM values estimated by Hovatta et al. (2012) and subtracted from their own initial RM maps are also given in Table 1.

We tested the derived shifts between images at the different frequencies by making spectral-index maps after applying these shifts in order to verify that they did not show any spurious features that could be due to residual misalignment. We also checked for broad consistency with the shifts derived earlier for these same data (Pushkarev et al. 2012). Hovatta et al. (2012) also noted that their analyses confirmed that the appearance of the spectral-index maps provides a good test of the correctness of the relative alignment of the images at the various frequencies.

Hovatta et al. (2012) made RM maps for a sample of 191 extragalactic radio sources, but due to the limits they imposed on their analysis of possible transverse RM gradients, they only were able to identify transverse RM gradients that satisfied their criteria in four sources. We visually inspected each of their 191 maps and identified for analysis 38 sources that showed possible transverse RM gradients by eye. For each of these, we reconstructed the RM maps using the methods described above and took RM slices in any region potentially displaying transverse RM gradients, applying the new error estimation approach of Hovatta et al. (2012) to estimate the RM uncertainties in individual pixels as input to our estimate of the significances of any RM gradients analyzed.

We detected statistically significant, monotonic transverse RM gradients across the jets of 18 of the 38 sources investigated, which are considered further below. The main factors contributing to the larger number of such transverse RM gradients we were able to detect, compared to the much smaller number reported by Hovatta et al. (2012), was the exclusion by Hovatta et al. (2012) of transverse RM gradients arising within one beam width of the core, and spanning less than 1.5 beam widths across the jet.

3. Results

This paper represents the culmination of a series of studies carried out by Gabuzda et al. (2014, 2015a, 2017). Here, we present the results of a reanalysis of data used to produce the RM images previously published by Hovatta et al. (2012), based on VLBA data at 8.1, 8.4, 12.1 and 15.3 GHz, together with an overall statistical analysis for the collected results for transverse RM gradients across parsec-scale RM jets.

Our analysis of the 38 candidate AGNs with transverse RM gradients from among the overall sample of 191 sources from the study of Hovatta et al. (2012) indicated that 18 of these AGNs have firm, monotonic transverse RM gradients (significances of 2.8σ or greater, corresponding to a probability of occurring by chance of no more than 0.5%). Figure 1 presents 8.1-GHz intensity maps made with the nominal, naturally weighted elliptical beams with the corresponding RM distributions superposed (left), the corresponding intensity and RM maps made using equal-area circular beams (middle), and slices taken along the lines drawn across the RM distributions in the middle panels (right). These maps are all based on the 8.1–15.2 GHz data of Hovatta et al. (2012); information about the map peaks and bottom contours and the beam sizes is given in Table 2.

All 18 of these AGNs display statistically significant transverse RM gradients across their jets, consistent with these jet **B** fields having significant toroidal components, possibly associated with helical jet **B** fields. Transverse RM gradients are detected in 13 of these AGNs for the first time, while the remaining 5 cases correspond to AGNs in which transverse RM gradients have been observed previously.

We note that, in large source samples, a small number of spurious 3σ gradients can appear purely by chance. In a sample of 191 sources, with the probability that a 3σ gradient is spurious being no larger than about 1%, we would expect no more than one or two such cases. Thus, it is possible that one or two of the 18 transverse RM gradients we have identified are spurious; thus, the vast majority of the statistically significant transverse RM gradients we have detected in these data represent real physical gradients, and the number of possible spurious gradients is too small to affect our overall results.

4. Discussion

A list of our 13 new and 5 confirmed transverse RM gradients together with all other known statistically significant transverse RM gradients on parsec scales from the literature (based on 5–15 GHz and 8–15 GHz RM maps) is given in Table 3. We note that the other AGNs analyzed to obtain these collected results are contained in subsamples of the 191 AGNs considered by Hovatta et al. (2012), each containing no more than 40 AGNs, making it unlikely that a significant number of the gradients detected in those samples are spurious. Thus, we expect overall that at most two of the transverse RM gradients listed in Table 1 are spurious.

The key importance of these new results is that they appreciably increase the total number of AGNs in which firm transverse RM gradients have been found, raising this number to 52, enabling for the first time a reliable statistical analysis of the directions of these transverse RM gradients on the sky; that is, the directions of the jet currents implied by the toroidal **B** field components giving rise to the RM gradients. Five of these 52 sources show time variability in the directions of their transverse Faraday RM gradients, and so cannot be used straightforwardly in such

Table 3: Transverse RM Gradients

Source	Ref	Implied Current [†]	Comments
Firm, $\geq 2.8\sigma$ or confirmed			
0059+581	*	Out	Reversal
0133+476	*	Out	
0212+735	G17,*	In	Reversal
0256+075	G15b	In	
0300+470	G17	In	
0305+039	G17	In	
0333+321	G14	In	
0355+508	G15b	Out	
0403-132	*	In	Possible reversal
0415+379	G17	In	
0430+052	Go11	In	
0446+112	*	Out	
0552+398	*	In	
0716+714	M13	In	Reversal
0735+178	G15b	In	
0738+313	G14	Out	
0745+241	G15b	In	
0748+126	G15b	In	
0820+225	G15b	In	
0823+033	G15b	Out	
0834-201	*	Out	
0859-140	*	In	Reversal
0923+392	G14	In	Reversal
0945+408	G17	In	
0955+476	*	In	
1124-186	*	In	
1156+295	G15b	In	
1218+285	G15b	In	
1226+023	H12	Out	
1334-127	G15b	Out	
1502+106	G17	Out	
1504-166	*	In	
1611+343	G17,*	Out	
1633+382	G14	In	
1641+399	*,MG17	In	
1652+398	G15b	Out	
1749+096	G15b	In	
1749+701	M13	In	Reversal
1807+698	G15b	In	
1908-201	*	In	
2007+777	G15b	Out	
2037+511	G14	In	Reversal
2155-152	G15b	In	
2216-038	*	In	
2230+114	H12	In	
2345-167	G14	Out	
2351+456	*	In	
Significant RM Gradients Showing Time Variability			
0836+710	G14,MG17		
1150+812	G14,*		Possible reversal
1803+784	M09		
2005+403	G17,*		
2200+420	G17,MG17		

G14 = Gabuzda et al. 2014; G15b = Gabuzda et al. 2015b; G17 = Gabuzda et al. 2017; Go11 = Gómez et al. 2011; H12 = Hovatta et al. 2012; M09 = Mahmud et al. 2009; M13 = Mahmud et al. 2013; MG17 = Motter & Gabuzda 2017; * = this paper;

[†] Current corresponding to direction of innermost gradient is given for sources displaying reversals.

an analysis (we will discuss a possible origin for this variability below).

Among the 47 sources for which the available data show no evidence of time variability, the transverse RM gradients in 33 imply inward jet currents and those in the remaining 14 outward

jet currents. The probability of this asymmetry coming about by chance can be estimated using a simple analysis based on a binomial probability distribution: the probability of obtaining N_{in} inward currents and N_{out} outward currents in a total of $N_{in} + N_{out}$ jets by chance, if the probabilities of each of these jets having inward or outward current are both equal to 0.5, is

$$P_{chance} = \frac{1}{2^{(N_{in}+N_{out})}} \frac{(N_{in} + N_{out})!}{N_{in}!N_{out}!}. \quad (3)$$

With $N_{in} = 33$ and $N_{out} = 14$, this yields a probability of 0.243%. However, to accurately determine the total probability of such an asymmetry in the number of inward and outward currents coming about by chance, we must determine the total probability of 33 or more of the 47 jets having inward current; summing all these individual probabilities using the formula above yields a total probability of 0.40%. This low probability testifies that this asymmetry is a real physical effect.

This asymmetry was in fact noted earlier by Contopoulos et al. (2009), but their analysis was marred by a lack of estimates of the significances for the 29 transverse RM gradients considered, which were found from a purely visual inspection of RM maps in the literature. This cast substantial doubt over those results. This has been remedied by the analysis of the collected results presented here: in the course of the analyses leading to the results listed in Table 3, the significances of all 29 potential RM gradients identified earlier by Contopoulos et al. (2009) by eye were checked: of these 29 RM gradients, 22 proved to be statistically significant, 5 to be not statistically significant, and 2 to be statistically significant but time variable. The fact that 24 of the 29 proved to be statistically significant simply reflects the fact that the human eye is a reasonably good 3σ gradient detector. In addition to clarifying which of the gradients considered earlier by Contopoulos et al. (2009) are robust, the results in Table 3, including those presented in this paper, have added another 28 cases, more than doubling the available statistics.

We note that the absolute values of the observed RMs will be affected by the local Doppler factor, however, it is physically implausible for this to give rise to systematic gradients in the observed RM across the jet. The Doppler factor depends on the intrinsic flow speed and the viewing angle, neither of which is expected to change systematically across the jet. An RM gradient could in principle be associated with a gradient in the electron density; however, electron-density gradients cannot give rise to the changes in the sign of the RM across the jets observed for a substantial number of the AGNs displaying transverse RM gradients. In addition, there is certainly no physically plausible picture in which electron-density gradients could have a preferred direction across the jet, whereas this comes about naturally if there is a preferred direction for the jet current (i.e. for the jet toroidal **B**-field component).

Thus, it is now possible to assert with confidence that the orientations of the toroidal **B** field components of AGN jets on the sky are not random, and that inward currents are considerably more common in AGN jets on parsec scales than outward currents.

This result would be extremely interesting even on its own; however, it becomes truly intriguing when combined with the results of Christodoulou et al. (2016) and Knuettel et al. (2018), which indicate a strong, highly significantly significant predominance of *outward* currents implied by transverse RM gradients on decaparsec-to-kiloparsec scales: 11 of 11 such gradients with significances $\geq 3\sigma$ correspond to outward currents. The probability of this coming about by chance is only $\approx 0.05\%$. At first glance, it might seem impossible to have predominantly inward

jet currents on parsec scales, but outward jet currents on larger scales. However, here we must recall that these currents can be distributed across the cross section of the jet and surrounding space, and the effect that we are using to trace these currents is the observed transverse RM gradients.

In fact, as was proposed earlier (Contopoulos et al. 2009, Mahmud et al. 2013) these collected results are consistent with a **B**-field configuration forming a nested helical-field structure, with one region of helical field inside the other and with the two having oppositely directed toroidal components. The orientation of the inner toroidal component corresponds to inward currents along the jet, and that of the outer toroidal component to outward currents along the jet direction, as shown schematically in Fig. 2. This forms a system of currents and fields similar to that of a co-axial cable, with inward current along the center of the cable and outward current in a more extended sheath. Both of the regions of helical field contribute to the overall observed Faraday rotation; the inner region of helical field makes the dominant contribution on parsec scales, while the outer region of helical field makes the dominant contribution beyond a few tens of parsec from the jet base. Changes in the conditions in different regions along and across the jet with time could also explain the changes in the direction of the significant transverse RM gradients observed in some sources as being due to changes in whether the inner or outer region of helical **B** field dominates the overall Faraday-rotation integral at that location.

The inner and outer regions of helical field correspond to the inner and outer sections of **B** field loops that have both been “wound up” by the differential rotation of the central black hole and its accretion disk. The distance at which each region dominates the observed transverse Faraday rotation gradients can be related to the scale on which the inner and outer (relative to the jet axis) sections of the initial loops of field are effectively “wound up” by the rotation (Christodoulou et al. 2016). The current flows inward along the jet axis and outward in a more extended region surrounding the jet, closing in the kiloparsec-scale lobes and in the accretion disk.

The physical origin of this system of fields and currents is key to understanding the launching and propagation of astrophysical jets. It is also important to note that the detection of statistically significant transverse Faraday rotation gradients even out to kiloparsec scales (Gabuzda et al. 2015a, Christodoulou et al. 2016, Knuettel et al. 2018) demonstrates that an ordered helical or toroidal field component at least partially survives along the entire length of the jet, though it may be masked by turbulence in some regions.

It has already been pointed out (Contopoulos et al. 2009, Christodoulou et al. 2016) that the configuration described above is in fact predicted by a “cosmic battery” model, in which currents are generated in the accretion disk by the action of the Poynting–Robertson effect, giving rise to a correlation between the direction of the poloidal **B** field that is “wound up” and the direction of rotation of the accretion disk. This correlation leads to a preferred orientation for the resulting toroidal **B** field component, which corresponds to an inward current along the jet axis. This mechanism produces loops of magnetic field whose inner and outer parts relative to the jet axis have opposite poloidal field directions, giving rise to opposite toroidal field directions when they are wound up — a nested helical-field configuration such as has been proposed as a way of explaining the opposite preferred directions for the observed transverse RM gradients (toroidal **B**-field components) on parsec and decaparsec-kiloparsec scales.

5. Conclusions

We identify 13 new cases and confirm another 5 previously identified cases of statistically significant transverse RM gradients across the parsec-scale jets of AGNs in the sample initially analyzed by Hovatta et al. (2012). According to the Monte Carlo simulations of Hovatta et al. (2012) and Murphy & Gabuzda (2013), the probability of a $\approx 3\sigma$ RM gradient arising by chance in RM maps based on VLBA snapshot data at the frequencies considered here is no more than about 1%; we accordingly expect no more than ≈ 2 of these gradients to be spurious, since the total sample contains 191 AGNs.

A statistical analysis of the collected results for the 47 AGNs that have now been found to display statistically significant transverse RM gradients on parsec scales indicates a clear preference for a predominance of inward jet current on these scales. The probability that this asymmetry has come about by chance is only $\approx 0.40\%$. In contrast, the collected results for AGNs displaying statistically significant transverse RM gradients on larger (decaparsec-to-kiloparsec) scales show a distinct predominance of outward currents, with an even lower probability of this asymmetry arising by chance (Christodoulou et al. 2016, Knuettel et al. 2018). These results can be understood if the overall systems of currents associated with AGN jets are similar to those of a coaxial cable, with an inward current running down the center of the jet and an outward current flowing in a more extended sheath-like region around the jet. This suggests the action of a “battery” mechanism that is determining the direction of these currents (or equivalently the direction of their associated toroidal **B**-field components); one possibility is the mechanism described by Contopoulos et al. (2009) and Christodoulou et al. (2016).

A very interesting question that remains to be addressed is why a sizeable minority of the 47 AGNs listed in Table 2 have transverse RM gradients on parsec scales whose directions imply outward rather than inward currents. One possibility is that the transition from dominance of the inner to dominance of the outer region of helical **B** field expected in the cosmic-battery model occurs on smaller angular scales than those probed by the available observations in these sources. It is also possible that the physical conditions in the accretion disks of some AGNs are less conducive to efficient operation of the battery mechanism; in this case, some fraction of the observed RM gradients would in fact have random directions, with an excess corresponding to inward current arising due to the operation of some mechanism that facilitates the development of inward jet currents. It may also be that the direction of the jet current is also affected by other factors, such as Hall currents, as was suggested by König (2010). Finally, the numerical computations of Koutsantoniou and Contopoulos (2014) suggest that the cosmic battery described above may operate in reverse when the central black hole rotates at more than about 70% of its maximal rotation; in such a case, the inner edge of the accretion disk would be close enough to the black hole horizon for the effect of the rotation of space–time to dominate over the effect of the disk’s rotation, leading to a reversal in the direction of the radiation force on the electrons in the accretion disk in the toroidal direction. Future studies aimed at characterizing the properties of the minority of AGNs whose transverse RM gradients imply outward currents on parsec scales and possible differences from the properties of the majority of AGNs whose jets are observed to have inward currents are certainly of interest.

Whether or not the particular “cosmic battery” model described above is indeed operating in the jet–accretion disk sys-

tems of AGNs has not been settled. However, our results have now yielded firm evidence that many — possibly all — AGN jets have inward currents along their axes and outward currents in a more extended region surrounding the jets. This provides fundamental information about the conditions leading to the formation and launching of the jets, as well as key input to theoretical simulations of astrophysical jets. It also indicates that astrophysical jets are fundamentally electromagnetic structures, which must be borne in mind when interpreting observed features in the distributions of both their intensity and linear polarization.

Acknowledgements. We thank the referee for his/her clear and pertinent comments, which have helped improve the overall clarity of this paper.

References

- Blandford, R. D. 1993, in *Astrophysical Jets* (Cambridge: Cambridge Univ. Press), p. 26
- Blandford, R. D. & Königl A. 1979, *ApJ*, 232, 34
- Burn, B. J. 1966, *MNRAS*, 133, 67
- Christodoulou, D. M., Gabuzda, D. C., Knuettel, S., Contopoulos, I., Kazanas, D. & Coughlan, C. P. 2016, *A&A*, 591, 61
- Cobb, W. K. 1993, PhD thesis, Brandeis University
- Contopoulos, I., Christodoulou, D. M., Kazanas, D., & Gabuzda, D. C. 2009, *ApJL*, 702, L148
- Croke, S. M. & Gabuzda, D. C. 2008, *MNRAS*, 386, 619
- Gabuzda, D. C., Knuettel, S. & Bonafede, A. 2015a, *A&A*, 583, 96
- Gabuzda, D. C., Knuettel, S. & Reardon, B. 2015b, *MNRAS*, 450, 2441
- Gabuzda, D. C., Reichstein, A. R., & O’Neill E. L. 2014, *MNRAS*, 444, 172
- Gabuzda, D. C., Roche, N., Kirwan, A., Knuettel, S., Nagle, M. & Houston, C. 2017, *MNRAS*, 472, 1792
- Gómez, J. L., Roca-Sogorb, M., Agudo, I., Marscher, A. P. & Jorstad, S. G. 2011, *ApJ*, 733, 11
- Hovatta, T., Lister, M. L., Aller, M. F., Aller, H. D., Homan, D. C., Kovalev, Y. Y., Pushkarev, A. B. & Savolainen, T. 2012, *AJ*, 144, 105
- Königl, A 2010, *MNRAS*, 407L, 79
- Knuettel, S., Gabuzda, D. & O’Sullivan, S. P. 2018, in *Polarised Emission from Astrophysical Jets, Galaxies*, 5 (4), 61 (<http://www.mdpi.com/2075-4434/5/4/61>).
- Koutsantoniou, L. & Contopoulos, I. 2014, *ApJ*, 794, 27
- Mahmud, M., Coughlan, C. P., Murphy, E. & Gabuzda D. C. 2013, *MNRAS*, 431, 695
- Mahmud, M., Gabuzda, D. C. & Bezrukovs, V. 2009, *MNRAS*, 400, 2
- Motter, J. C. & Gabuzda, D. C. 2017, *MNRAS*, 467, 2648
- Murphy E. & Gabuzda D. C. 2013, in *The Innermost Regions of Relativistic Jets and Their Magnetic Fields*, EPJ Web of Conferences, 61, 07005 (http://www.epj-conferences.org/articles/epjconf/abs/2013/22/epjconf_rj2013_07005/epjconf_rj2013_07005.html)
- Pacholczyk, A. G., *Radio Astrophysics* (W. H. Freeman, San Francisco, 1970)
- Perley, R. A., Bridle, A. H. & Willis, A. G. 1984, *ApJS*, 54, 291
- Pushkarev, A. B., Hovatta, T., Kovalev, Y. Y., Lister, M. L., Lobanov, A. P., Savolainen, T. & Zensus, J. A. 2012, *A&A*, 545, 113
- Simard-Normandin, M., Kronberg, P. P. & Button, S. 1981, *ApJS*, 45, 91
- Taylor, A. R., Stil, J. M. & Sunstrum, C. 2009, *ApJ*, 702, 1230
- Tchekhovskoy, A. & Bromberg, O. 2016, *MNRAS*, 461, L46
- Wardle, J. F. C. 2018, in *Polarised Emission from Astrophysical Jets, Galaxies*, in press 794, 27

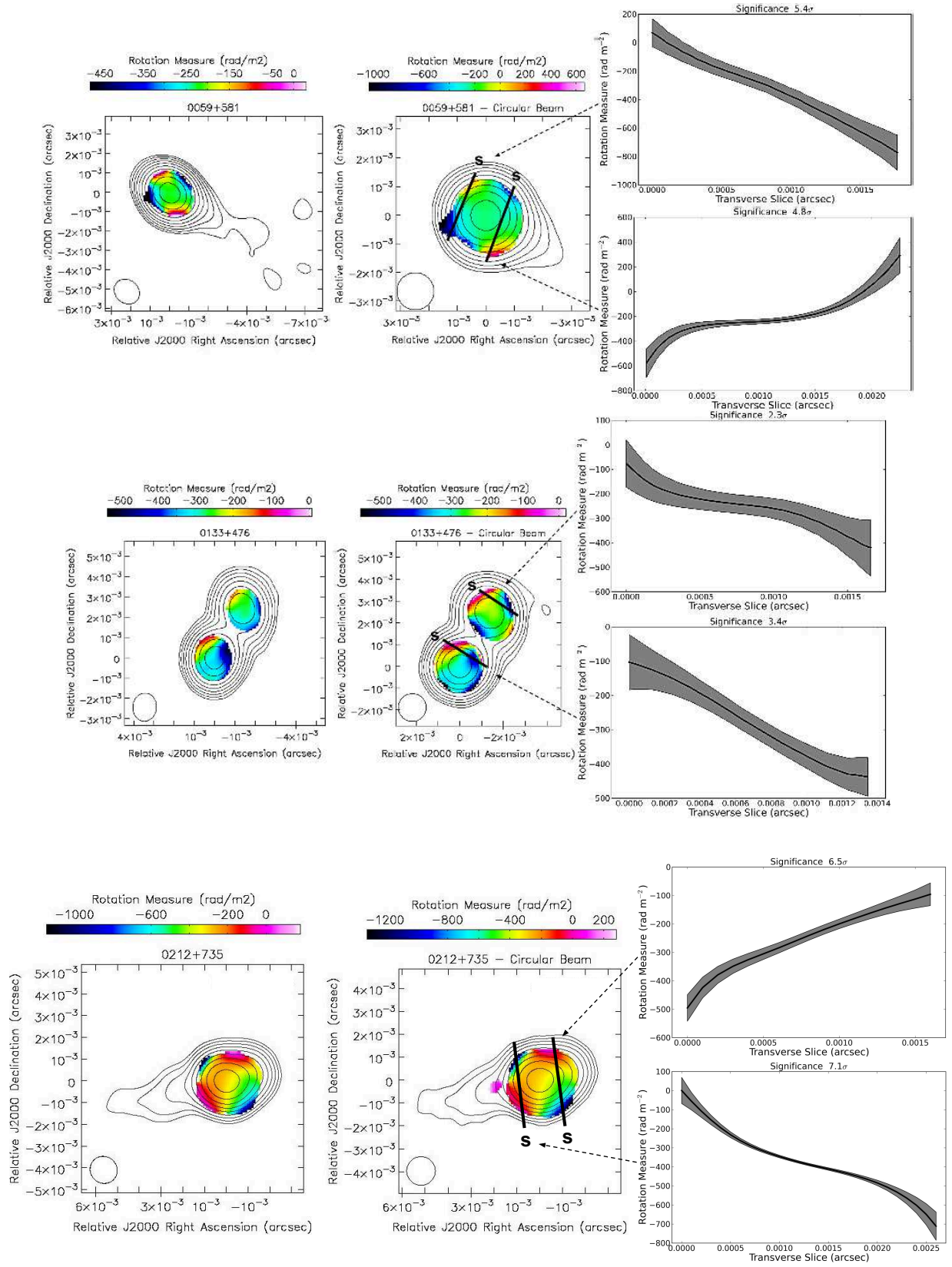


Fig. 1. 8.1-GHz intensity maps made with the nominal, naturally weighted elliptical beams with the corresponding RM distributions superposed (left), the corresponding intensity and RM maps made using equal-area circular beams (middle), and slices taken along the lines drawn across the RM distributions in the middle panels (right). These maps are based on the 8.1–15.2 GHz data of Hovatta et al. (2012); information about the map peaks, bottom contours, and the beam sizes is given in Table 2. Shown here are results for 0059+581 (top), 0133+476 (middle) and 0212+735 (bottom).

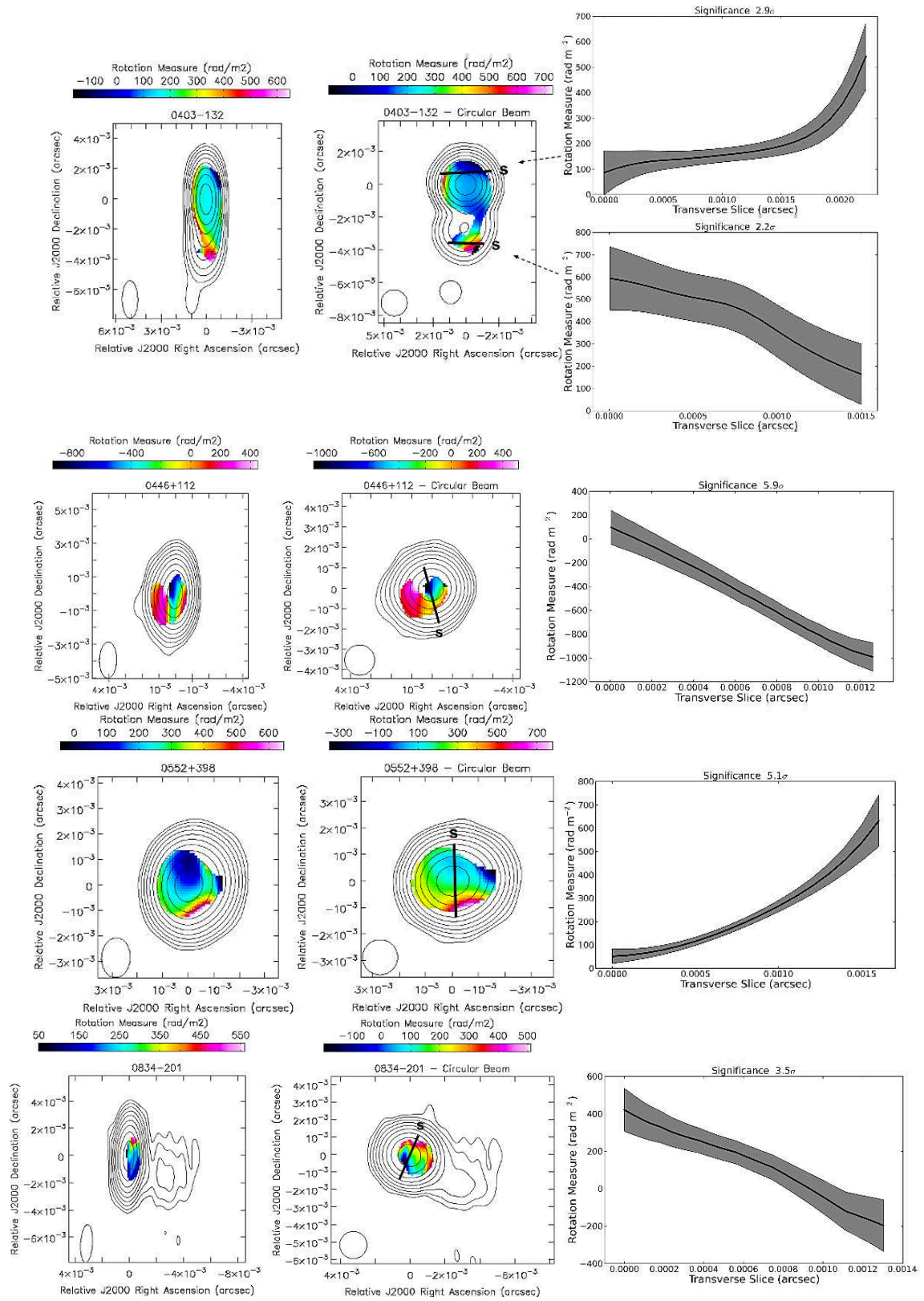


Fig. 1. Continued. Results for 0403-132, 0446+112, 0552+398 and 0834-201 (from top to bottom).

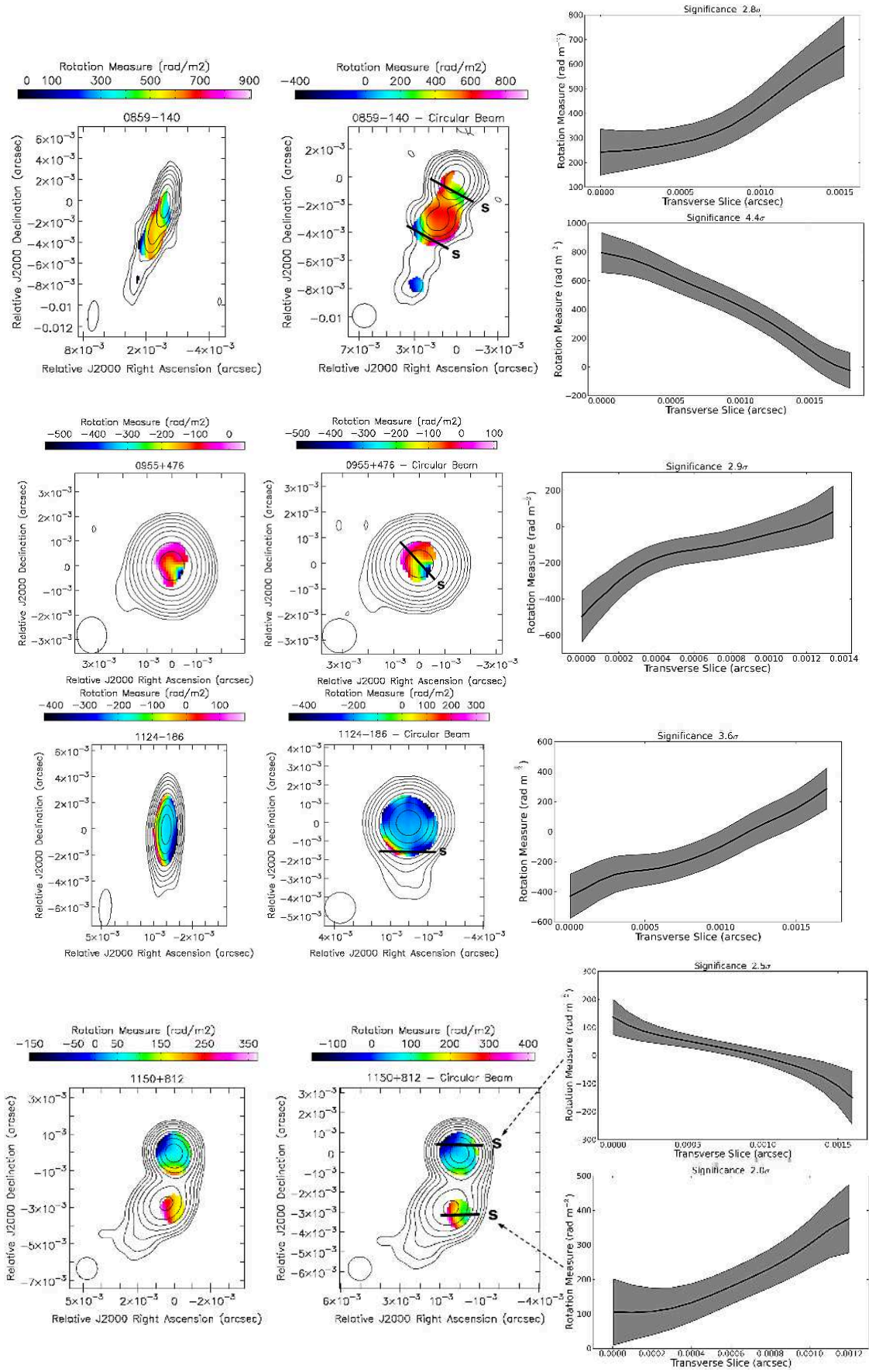


Fig. 1. Continued. Results for 0859–140, 0955+476, 1124–186 and 1150+812 (from top to bottom).

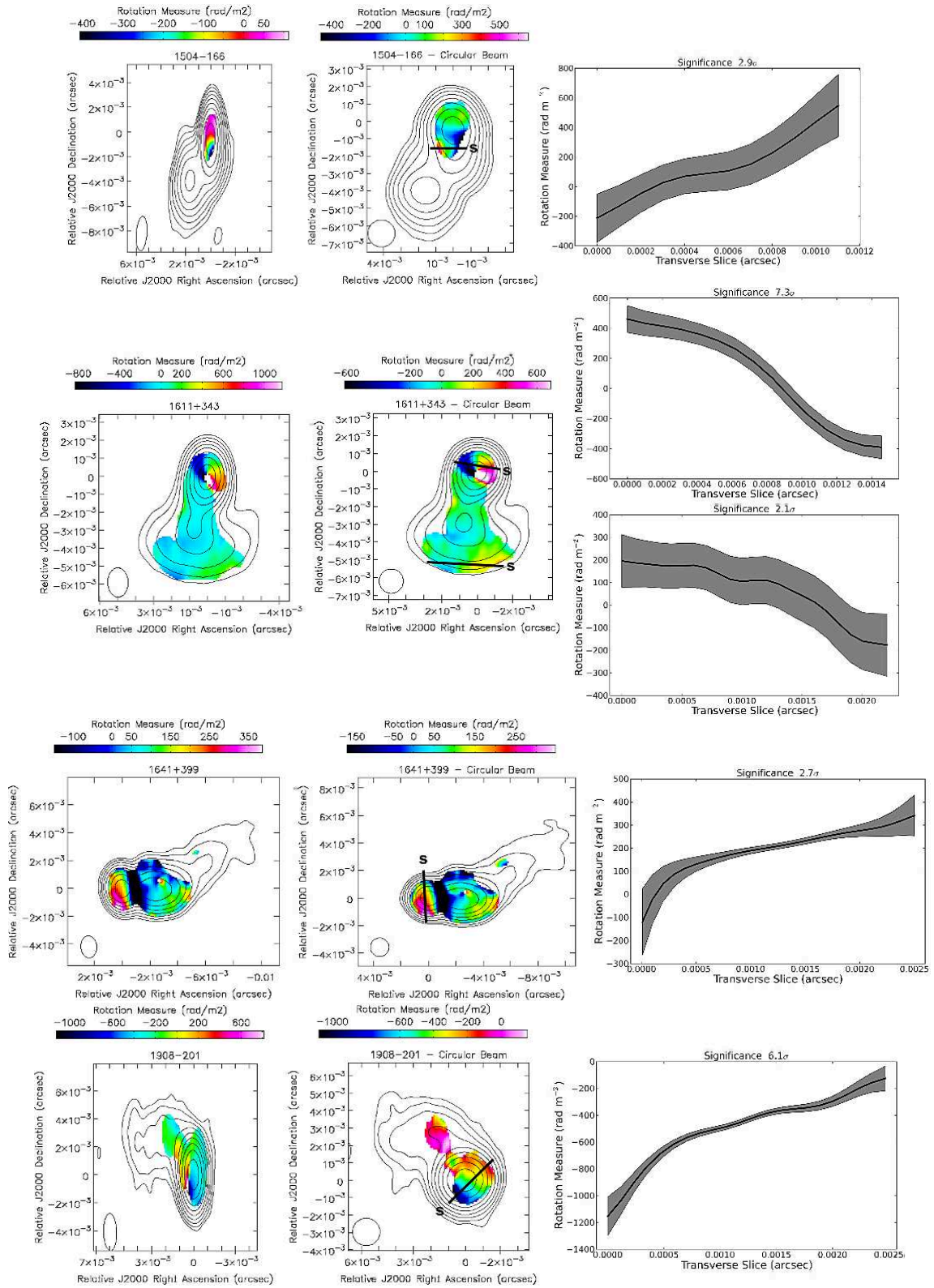


Fig. 1. Continued. Results for 1504-166, 1611+343, 1641+399 and 1908-201 (from top to bottom).

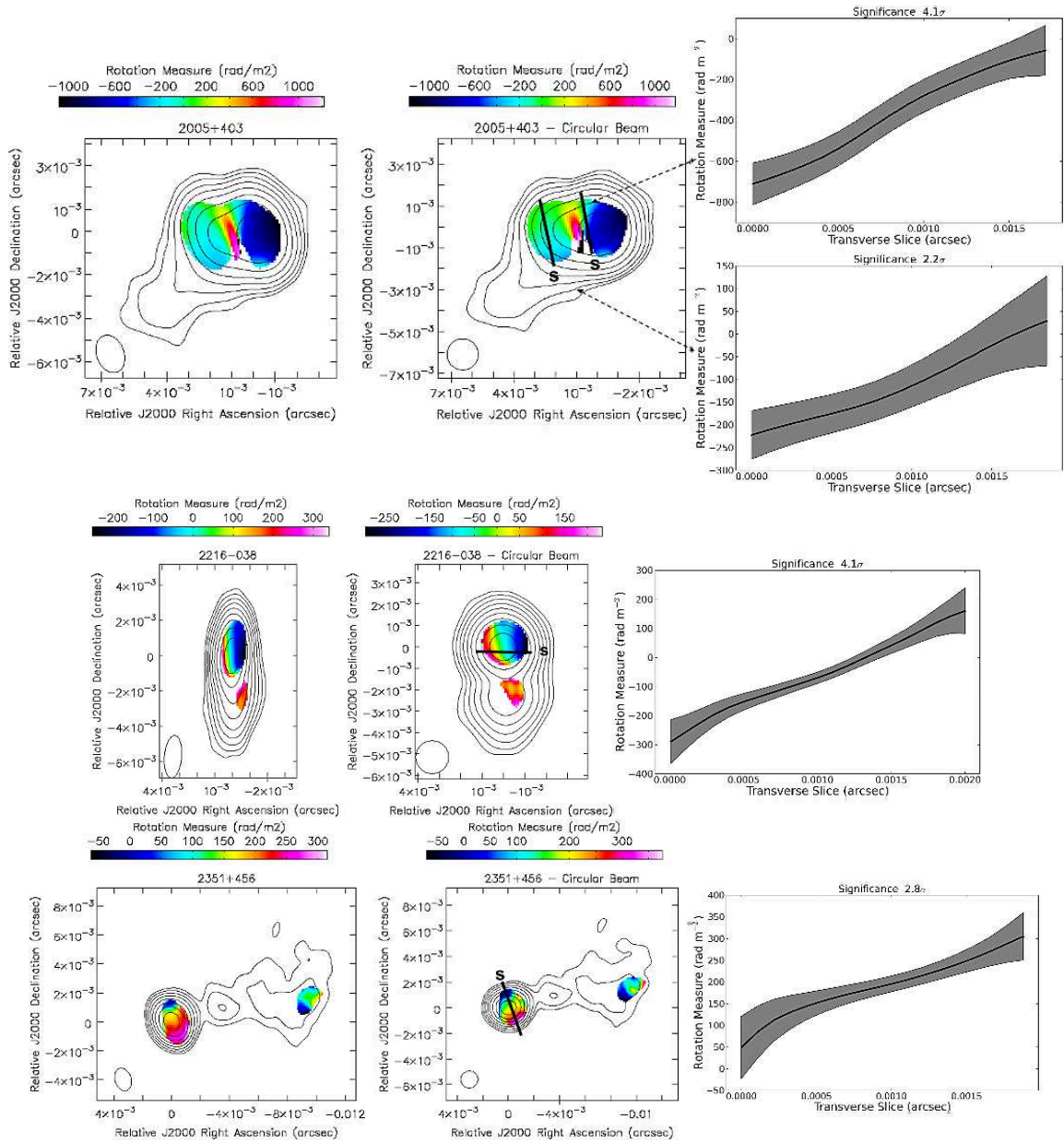


Fig. 1. Continued. Results for 2005+403 (top), 2216-038 (middle) and 2351+456 (bottom).

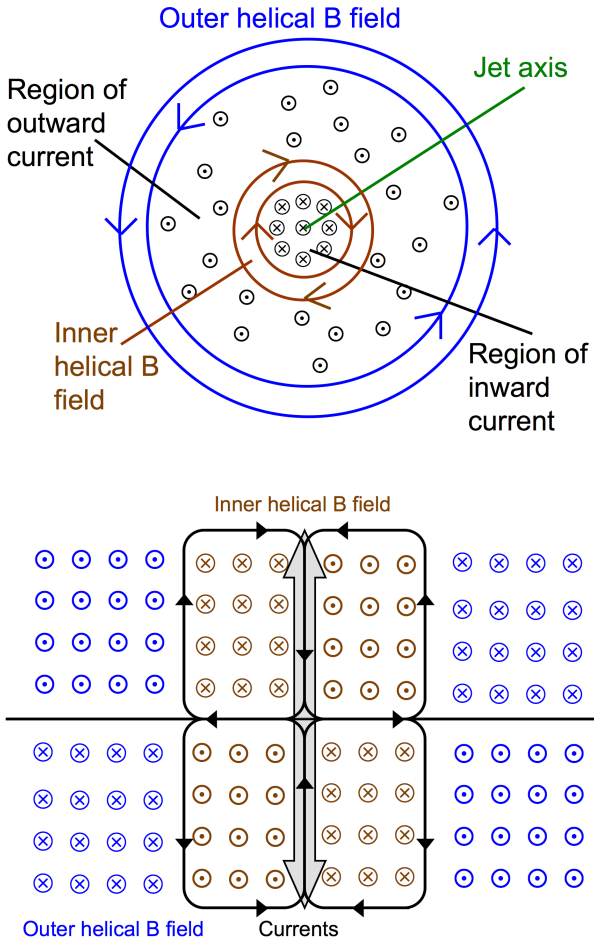


Fig. 2. Schematics of the system of \mathbf{B} fields and currents suggested by the collected data on transverse Faraday rotation gradients, as viewed from above (i.e., looking down the jet) (upper) and from the side (lower). The region of inner helical field is shown in brown, the region of outer helical field in blue, and the currents in black. The partially transparent gray arrows in the lower panel represent the jet outflow. A circled dot represents current or field oriented out of the page and a circled X current or field oriented into the page.